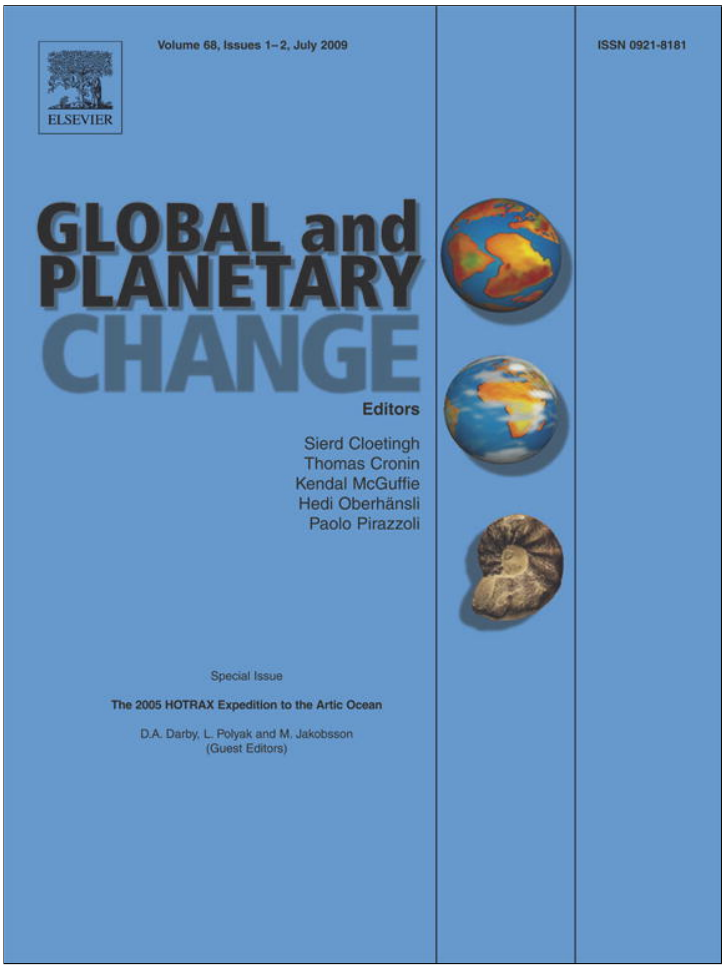

Global and Planetary Change 68 (2009) 85–99

Contents lists available at ScienceDirect

Global and Planetary Change

journal homepage: www.elsevier.com/locate/gloplacha

Paleomagnetic constraints on the Holocene stratigraphy of the Arctic Alaskan margin

Agathe Lisé-Pronovost [a,b,*], Guillaume St-Onge [a,b], Stefanie Brachfeld [c], Francesco Barletta [a,b], Dennis Darby [d]

[a] Institut des sciences de la mer de Rimouski (ISMER), 310 allée des Ursulines, Rimouski, QC, Canada G5L 3A1
[b] GEOTOP research center, QC, Canada
[c] Montclair State University, NJ, USA
[d] Dept. of Ocean, Earth, & Atmospheric Sciences, Old Dominion University, VA, USA

ARTICLE INFO

Article history:
Received 23 July 2008
Accepted 12 March 2009
Available online 31 March 2009

Keywords:
paleomagnetism
Arctic
Holocene
paleomagnetic secular variation
relative paleointensity
marine sediment

ABSTRACT

Two long Holocene piston cores (HLY0501-06JPC and -08JPC; herein after referred to as 6JPC and 8JPC) were raised from high sediment accumulation areas in the Arctic Alaskan margin in order to reconstruct the millennial- to centennial-scale behavior of Earth's magnetic field and to better constrain the regional chronostratigraphy of the Western Arctic. Paleomagnetic analyses using a u-channel cryogenic magnetometer (natural, anhysteretic and isothermal remanent magnetizations: NRM, ARM and IRM) and a vibrating sample magnetometer indicate that a strong and stable single component characteristic remanent magnetization carried by low coercivity pseudo-single domain (PSD) grains such as magnetite can be isolated in the postglacial unit of both cores, where the inclination values vary around the geocentric axial dipole (GAD) for the latitude of the coring sites and where the maximum angular deviation (MAD) values are generally lower than 5°. Apart from one interval in each core, all the derived relative paleointensity proxies (NRM/k_{LF}, NRM/ARM and NRM/IRM) yield similar results. NRM/IRM was used as the preferred proxy because, based on cross-spectral analysis, it is not coherent with its normalizer. Based on the comparison with paleomagnetic records from Western North America, the paleomagnetic and physical analyses indicate that both sedimentary sequences have recorded some of the first reliable Arctic high-resolution records of paleomagnetic secular variation (inclination and declination) and relative paleointensity during the Holocene. In addition, full vector paleomagnetic correlations (inclination, declination and relative paleointensity) were used to constrain the chronology of core 6JPC, using core 8JPC and other previously published and independently dated sedimentary and volcanic records from Western North America. The Accelerator Mass Spectroscopy (AMS) radiocarbon-based postglacial chronology of core 8JPC indicates sedimentation rates higher than 300 cm/kyr on the continental shelf near Barrow Canyon from approximately 8000 to 5000 cal BP, followed by a major decrease in sediment deposition. In contrast, the postglacial deposition on the slope at core site 6JPC is relatively constant and sedimentation rates are nearly three times lower.

1. Introduction

The study of millennial-scale variation of the Earth's magnetic field recorded by sedimentary sequences is a means of better understanding the geomagnetic field high frequency behavior, and can be a very useful stratigraphic tool (e.g., Guyodo and Valet, 1996, 1999; Laj et al., 2000; Stoner and St-Onge, 2007). In the last few decades, an increasing number of Holocene paleomagnetic studies based on marine and lacustrine sediment sequences have been published. In an effort to further develop magnetostratigraphy as a regional dating tool, Holocene paleomagnetic reference curves have been constructed (e.g., Turner and Thompson, 1981; Snowball and Sandgren, 2002; Snowball et al., 2007; Lund and Banerjee, 1985; Verosub et al., 1986; Lund, 1996; Creer and Tucholka, 1982; Gogorza et al., 2000). In parallel, Korte and Constable (2005) developed a global geomagnetic field model (cals7k) based on spherical harmonic analysis. This model was calibrated with archeomagnetic (from volcanic rocks and fired artifacts) and paleomagnetic (from sedimentary sequences) data for the last 7 kyr and it has succeeded in reproducing some of the millennial- to centennial-scale dipole moment variability observed in the sediment sequences (Korte and Constable, 2006).

The observation of synchronous changes of the geomagnetic field, either inclination, declination and/or intensity at sites from the same area can lead to the identification of regional chronostratigraphic markers. For example, Barletta et al. (2008) recently observed several directional and paleointensity features that have the potential to be used as chronostratigraphic markers for Holocene sediments in the Western Arctic. Such markers are especially attractive in the Arctic, where dating is often complicated (see below). Due to their proximity

* Corresponding author.
E-mail address: agathe.lisepronovost@uqar.qc.ca (A. Lisé-Pronovost).

0921-8181/$ – see front matter © 2009 Elsevier B.V. All rights reserved.
doi:10.1016/j.gloplacha.2009.03.015

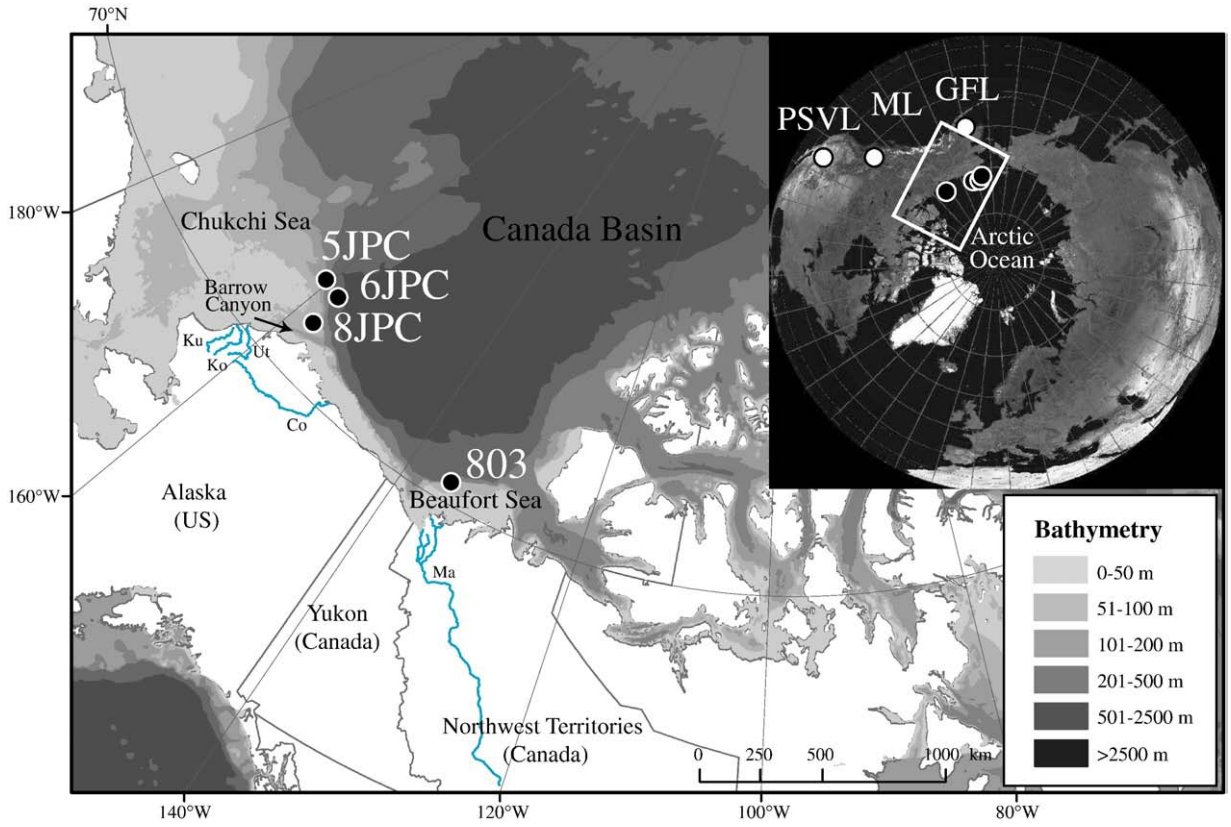

Fig. 1. Location of cores 8JPC and 6JPC in the Western Arctic Ocean as well as other high-resolution Western North American records cited in the text: 5JPC and 803 (Barletta et al., 2008), PSVL (paleosecular variation from lava flows; Hagstrum and Champion, 2002), ML (Mara Lake; Turner and Thompson, 1981) and GFL (Grandfather Lake; Geiss and Benerjee, 2003). Also shown are the rivers discussed in the text. Abbreviations: Ut — Utukok River, Ko — Kokolik River, Ku — Kukpowruk River, Co — Colville River, Ma — Mackenzie River.

to the North Magnetic Pole, the high latitude sites have the potential to record higher amplitude directional changes than the lower sites. Unfortunately, only a handful of paleomagnetic studies covering the Holocene period have been published from northern high latitude sites (>60°N) (Andrews and Jennings, 1990; Frank et al., 2002; Snowball and Sandgren, 2002; Geiss and Banerjee, 2003; Nowacyzk et al., 2001; Snowball and Sandgren, 2004; Snowball et al., 2007; Stoner et al., 2007; Barletta et al., 2008) and only a subset of these present the full paleomagnetic vector. Because high sedimentation rate sites are found on the continental shelves and slopes of Arctic marginal seas (Darby et al., 2006), these sites are key areas to address the millennial- to centennial-scale geomagnetic field variability for the Holocene.

The prerequisite for a paleoclimatic study based on a sedimentary sequence is the establishment of a reliable age model in order to transform the depth scale into an age scale. Since the radiocarbon reservoir effect is often poorly constrained in the Arctic and since the datable material is often very rare, the chronostratigraphy of Arctic marine sediment sequences has always been a challenge. It is therefore optimal to combine dating methods. High-resolution magnetostratigraphy is a valuable tool to date sediment sequences in the absence of datable material (e.g., Mackereth, 1971; Saarinen, 1999; St-Onge et al., 2004) or to independently support and improve a chronostratigraphy based on radiocarbon dating (e.g., Creer and Tucholka, 1982; Andrews et al., 1986; Kotilainen et al., 2000; Stoner et al., 2007). Reconstructing the geomagnetic field variability in the Arctic could therefore provide important stratigraphic constraints where traditional dating techniques are often limited. In this paper, we present the full vector paleomagnetic records (inclination, declination and relative paleointensity) of two long Holocene piston cores in order to constrain the stratigraphy of the Arctic Alaskan margin and to bring insights on the identification of possible regional chronostratigraphic markers.

2. Regional setting

The two studied jumbo piston cores were recovered from the Arctic Alaskan margin in the Eastern Chukchi Sea (Fig. 1). A distinct submarine feature in the area is the Barrow Canyon, a major pathway for dense Pacific water inflow from the Bering Strait (Pickart et al., 2005) and for sediment loaded waters moving from the continental shelf (Weingartner et al., 1998) toward the continental slope and the Canada Basin. In the present oceanographic conditions, upwelling events of intermediate-depth Atlantic waters from the Canada Basin into the Barrow Canyon have been observed episodically (Pickart et al., 2005).

Since the marine transgression (from about 12 000 cal BP on the Chukchi shelf; Keigwin et al., 2006) associated with the last deglaciation, the major sediment sources on the Arctic Alaskan margin come from river discharge, coastal erosion and redistribution of sediment by ice drift. Northern North American rivers bringing sediment at the Arctic Alaskan margin are found from the Beaufort Sea to the Bering Sea. The Colville River in Alaska (USA) and the Mackenzie River in the Northwest Territories (Canada) are major rivers forming deltas in the Western Arctic Ocean. However, smaller rivers located in Northwest Alaska (Utukok, Kokolik and Kukpowruk Rivers; Fig. 1) are reaching Barrow Canyon through a network of submarine paleochannels and would have been an important sediment source to the Northeast Chukchi Sea during the last deglaciation (Hill and Driscoll, 2008). Due to the present hydrodynamic conditions, most of the Chukchi shelf is the area of net seafloor erosion or non-deposition, whereas fine-grained sediments are deposited in the valleys such as the Barrow Canyon and deeper on the slope (Phillips et al., 1988). Grains are also transported and released in the Chukchi Sea by sea ice (Darby, 2003; Darby and Bischof, 2004).

Table 1
Core location.

Core	Latitude (°N)	Longitude (°W)	Localisation	Water depth (m)	Length (m)
HLY0501-06JPC	72.69	157.03	Lower mid-slope	673	15.54
-06TC	"	"	"	"	1.03
HLY0501-08JPC	71.63	156.86	Continental shelf	90	13.96
-08TC	"	"	"	"	3.06

The last major lithostratigraphic marker on the Western Arctic margins is the lithological change associated with the transition from deglacial to marine Holocene environments (e.g., Darby et al., 1997; Polyak et al., 2007). Previous geophysical seafloor surveys and core descriptions from the Chukchi Sea have shown that brownish to olive gray, strongly bioturbated mud (postglacial sediments) overlay stiffer grayish, sometimes laminated mud containing ice rafted debris (glacial/deglacial sediments) in the Chukchi Sea (Philips et al., 1998; Keigwin et al., 2006; Polyak et al., 2007). Similarly, Barletta et al. (2008) described a piston core from the Chukchi Sea with about 12 m of postglacial olive gray mud overlying glacial/deglacial sediments.

3. Materials and methods

3.1. Coring sites

Two long jumbo piston cores (HLY0501-06JPC and HLY0501-08JPC, hereinafter referred as cores 6JPC and 8JPC, respectively; Table 1) from the Arctic Alaskan margin were collected on board the USCGC Healy as part of the 2005 Healy-Oden Trans-Arctic Expedition (HOTRAX). The Alaskan margin coring sites were selected using the hull-mounted 3.5 kHz subbottom profiler and the 12 kHz multibeam bathymetric sonar for the areas of significant apparent thickness (>10 m) of Holocene sediments, as previously observed in the area (Phillips et al., 1988; Keigwin et al., 2006), and for the absence of erosional features or sediment deformation by mass movements. Core 8JPC was raised from the continental shelf (90 m water depth) near the Barrow Canyon, while core 6JPC was collected ~100 km northwards in the lower mid-slope (673 m water depth; Table 1; Fig. 1).

3.2. Physical analysis

On board, the piston cores were analyzed with a GEOTEK™ Multi Sensor Core Logger for the determination of wet bulk density (by gamma-ray attenuation) and low-field volumetric magnetic susceptibility (k_{LF}) at 1 cm intervals, then split and described. k_{LF} is mainly proportional to the ferrimagnetic mineral concentration. However, k_{LF} increases with paramagnetic material when the concentration of ferrimagnetic material is low and with the addition of superparamagnetic (<0.03 μm) and large (>10 μm) magnetite grains (e.g., Thompson and Oldfield, 1986; Stoner and St-Onge, 2007). In the laboratory, the cores were photographed with a high-resolution digital camera and sampled with u-channels (u-shaped plastic liners of 2×2 cm cross-section and up to 1.5 m length).

The u-channels were then passed through a CAT-scan (Computerized Axial Tomography Scan) at the *Institut national de la recherche scientifique, Centre Eau Terre Environnement* (INRS-ETE) in Quebec city, Canada, in order to visualize the sedimentary structures and assess possible core deformation. The computed tomography (CT) numbers were extracted, primarily reflecting changes in bulk density with a 1-mm downcore resolution (St-Onge et al., 2007).

3.3. Paleomagnetic analysis

Paleomagnetic data were acquired at 1 cm intervals on u-channel samples using a 2G Enterprises™ cryogenic magnetometer and pulse magnetizer module (for Isothermal Remanent Magnatization, IRM) at the Paleo and Environmental Magnetism Laboratory at the *Institut des sciences de la mer de Rimouski* (ISMER), Canada. The response function of the magnetometer pick-up coils integrates measurements over ~4.5 cm (Weeks et al., 1993). To eliminate the edge effect associated with this response function, the first and last 5-cm data of each u-channel were excluded.

The natural remanent magnetization (NRM) was measured first using stepwise alternating field (AF) demagnetization at peak fields from 0 to 70 mT with 5 mT increments. Inclination and declination of the characteristic remanent magnetization (ChRM) were calculated by a least-square line-fitting procedure (Kirschvink, 1980) using the Mazaud (2005) software with AF demagnetization steps from 20 to 70 mT (11 steps). An anhysteretic remanent magnetization (ARM) was then induced at peak AF of 100 mT with a 0.05 mT direct current (DC) biasing field and subsequently demagnetized and measured at 0 mT and from 10 to 70 mT with 5 mT steps. An isothermal remanent magnetization (IRM) was imparted with a DC field of 0.3 T and subsequently demagnetized and measured at 0 mT, from 10 to 60 mT with 5 mT steps and at 70 mT. Similarly, a second IRM (corresponding to a Saturated Isothermal Remanent Magnetization, SIRM) was imparted with a higher DC field of 0.9 T and then demagnetized and measured at 0 mT, 10 mT, from 20 to 50 mT with 5 mT steps, at 60 mT and 70 mT. The arithmetic mean of each magnetic remanence (NRM, ARM, IRM and SIRM) for the demagnetization steps 25 to 50 mT (6 steps) is presented in Fig. 3.

Hysteresis properties were measured on pilot samples from core section breaks using a Princeton Measurements Corp™ vibrating sample magnetometer (VSM-3900-04C) at 10 mT increments with a maximum field of 1 T at Montclair State University in New Jersey, USA, in order to help constrain the magnetic mineralogy and granulometry. The following values were derived from the hysteresis curves: the coercivity of magnetic minerals (Hc), the coercivity of remanence (Hcr), the saturation magnetization (Ms) and the saturation remanence (Mrs).

All laboratory-induced magnetizations are dependant on the concentration of magnetic material present in the sample, but each type of magnetization activates a specific group of magnetic grains. Alone or normalized by another magnetic parameter, the different magnetizations are thus useful to characterize variations in magnetic mineralogy and granulometry (e.g., King et al., 1982; Thompson and Oldfield, 1986; Brachfeld and Banerjee, 2000; Maher et al., 1999; Peters and Dekkers, 2003; Stoner and St-Onge, 2007). SIRM normalized by the magnetic susceptibility (k_{LF}) is an indicator of the magnetic grain size, with smaller values denoting coarser magnetic grains (Thompson and Oldfield, 1986). In addition, a diagram of k_{LF} vs. SIRM (Thompson and Oldfield, 1986) is also used in this paper to estimate the magnetic grain size. Despite the fact that this plot is based on pure magnetite for calibration, it is often used in paleomagnetism to estimate the magnetic grain size (e.g., Stockhausen and Zolitschka, 1999; Nowaczyk et al., 2003; Gogorza et al., 2004). k_{ARM} is calculated by dividing the ARM by the strength of the DC field applied and is also used as a magnetic grain size indicator when divided by k_{LF}, where k_{ARM}/k_{LF} is inversely proportional to the magnetic grain size if the magnetic mineralogy is mainly magnetite (King et al., 1982). Finally, $IRM_{0\ mT}$ 0.3 T normalized by $IRM_{0\ mT}$ 0.9 T (pseudo S-ratio) is an indicator of the magnetic mineralogy, with values close to 1 denoting low coercivity minerals such as magnetite (e.g., St-Onge et al., 2003). The median destructive field (MDF) is the required peak field to reduce the initial magnetic remanence by half. The MDF is a magnetic mineralogy indicator depending on the coercivity of magnetic minerals and on the magnetic grain size (Dankers, 1981).

3.4. Radiocarbon analysis

Accelerator Mass Spectroscopy (AMS) radiocarbon measurements were performed on 9 mollusk shells (core 8JPC, Table 2) and on benthic foraminifers (core 6JPC, Table 2) at the Lawrence Livermore

Table 2
Radiocarbon dates from cores 6JPC and 8JPC.

Core	Depth (cm)	Adjusted depth (cm)	Dated material	Lab number	AMS ^{14}C age (yr BP)	Calibrated age[a] (cal BP)
HLY0501-06JPC	770–772	850–852	Benthic forams	CAMS135962	7690 ± 180	7790 (8160) 8520
	878–880	958–960	Benthic forams	AA74466	12 375 ± 60	13,710 (13 850) 13,980
HLY0501-08JPC	51	102	Bivalve *Macoma*	AA66974	3216 ± 37	2900 (3030) 3160
	130	181	Bivalve *Astarte*	CAMS137887	4590 ± 30	4700 (4790) 4880
	327	378	Bivalve *Nuculana*	CAMS137888	5210 ± 30	5480 (5560) 5640
	510	561	Bivalve *Macoma*	AA66975	5309 ± 79	5530 (5710) 5880
	789	840	Bivalve *Macoma?*	CAMS137889	5995 ± 35	6300 (6400) 6500
	851	902	Bivalve	CAMS137890	6110 ± 40	6430 (6540) 6650
	1116	1167	Bivalve	CAMS137378	7285 ± 35	7660 (7750) 7840
	1150	1201	Gastropode *Natica*?	AA66976	7760 ± 51	8110 (8230) 8350*
	1153	1204	Bivalve	CAMS137891	7415 ± 35	7790 (7880) 7960

[a] The conventional ages were calibrated with the CALIB5.0.2 (Stuiver et al., 2005) online calibration software using the Hughen et al. (2004) dataset and assuming a ΔR value of 0 (see text for details). The first and last ages represent the 2σ cal age range rounded to the nearest tens, whereas the ages in parentheses are the average age rounded to the nearest tens. * = excluded age.

National Laboratory's Center for Accelerator Mass Spectroscopy (LLNL-CAMS) and at the NSF-Arizona Accelerator Mass Spectroscopy Laboratory. The dates are reported using Libby's half-life and corrected for natural and sputtering fractionation ($\delta^{13}C = -25‰$ vs. VPDB). To convert the ^{14}C ages to calendar years, the dates were calibrated using the CALIB5.0.2 online calibration software (Stuiver et al., 2005), assuming a ΔR of 0. The calibrated ages are reported at the 2σ confidence level. Based on paleomagnetic data, a ΔR of 0 was recently shown to be appropriate for a nearby Arctic Alaskan margin core (Barletta et al., 2008). Nonetheless, uncertainties remain about the reservoir ages in the Western Arctic and therefore ages calibrated using a ΔR of 0 at sites where there is a possible Pacific component (e.g., shallower waters on the Alaskan margin; core 8JPC) should be considered as maximal ages.

4. Results

4.1. Core stratigraphy

Correlation of the physical and magnetic parameters measured on the piston cores (JPC) and their companion trigger weight cores (TC) suggests that 51 cm and 80 cm of sediments were lost due to coring at the top of cores 8JPC and 6JPC, respectively (Fig. 2). Compaction and/or stretching of the sediment due to piston and gravity coring are possible and the linear correlation coefficients are >0.71 (Fig. 2). The missing piston core sediments were taken into account and all depths hereinafter are expressed as adjusted depth if not otherwise specified. Because of significant sediment disturbances in the u-channel sampled from the trigger weight core 6TC, only measurements from the whole core (i.e. MSCL measurements) were used for correlation purposes of cores 6JPC and 6TC. A higher sediment lost (147 cm) at the top of core 6JPC is also possible and suggested by the diffuse spectral reflectance data (Ortiz et al., 2009-this issue). Even thought the depth scale is here presented using an adjustment of 80 cm, the possible higher sediment loss is also taken into account for the construction of core 6JPC age model (see Section 5.5).

A significant change in all the physical and magnetic parameters occurs at 935 cm in core 6JPC and 1230 cm in core 8JPC (Fig. 3). The top sedimentary unit of both cores is characterized by olive gray to dark olive gray fine mud to sandy mud. These sediments are typical of Arctic shelf postglacial sediments (e.g., Syvitski, 1991; Darby et al., 2006; Keigwin et al., 2006; Barletta et al., 2008). In addition, the sediment of this unit contains numerous black speckles which are likely iron sulfides. The basal sedimentary unit of core 8JPC is composed of gray to dark gray, stiff mud with sand and coarser grains, suggesting deposition in a glacial/deglacial regime and/or in nearshore environments during the sea level rise. In core 6JPC, the bottom of the top unit occurs at 935 cm and the first centimeter-scale dropstone is found above this transition, at 910 cm. Other dropstones are found at 1132 cm and 1290 cm, whereas ice rafted debris (IRD) are common from 1515 cm to the base of the core. Between 935 and 1515 cm, the sediment is composed of brown and olive gray mud laminations where sand and bioturbated contacts are found, which is typical of glaciomarine sediments (Syvitski, 1991). This interpretation is supported by an age of 13 850 cal BP at 858–860 cm (Table 2). From 1515 to 1535 cm, a yellowish brown sandy mud horizon with IRD is observed and contains a relatively higher concentration of high coercivity magnetic minerals as shown by a sharp decrease in the pseudo S-ratio (gray interval at the base of Fig. 3a). Below this horizon, the sediment becomes dark gray stiff sandy mud with the presence of IRD. The lowermost 50 cm contain patches with iron sulfides similar to postglacial sediment. Overall, the basal unit of core 6JPC contains multiple lithological changes and IRD, suggesting deposition in variable glacial/deglacial environments.

The following intervals were excluded from the dataset of core 6JPC postglacial unit due to sediment disturbance or incomplete filling of the u-channel as revealed by CAT-scan images and CT numbers: 121 to 127 cm, 332 to 355 cm, 385 to 400 cm and 446 to 456 cm. Similarly, the following intervals of core 8JPC postglacial unit were excluded: 170–194 cm, 485–507 cm and 1009–1018 cm. These unreliable intervals represent only 6.7% of the postglacial units (gray intervals in Figs. 3 and 5).

4.2. Natural remanent magnetization

A strong and stable characteristic remanent magnetization (ChRM) can be isolated in both cores between the AF demagnetization steps of 20–70 mT (Fig. 4). A weak viscous component is removed after a 15 mT or less demagnetization field. The mean postglacial $NRM_{0\ mT}$ is 0.058 ± 0.035 A/m for core 6JPC and 0.064 ± 0.042 A/m for core 8JPC.

4.3. Paleomagnetic directional data

The ChRM inclinations in the postglacial units of both cores vary around the calculated geocentric axial dipole (GAD) inclinations for the latitude of the coring sites (Fig. 5). The mean inclination value of the postglacial unit of core 6JPC (8JPC) is 81.4° ± 21.2° (79.3° ± 14.4°) and the GAD inclination value is 81.1° (80.6°). The ChRM declinations were corrected for rotation at section breaks and corrected for similar circular values (e.g., 0 and 360°) to obtain a continuous record. The declination data are relative and centered at zero since the coring was not azimuthally oriented.

The maximum angular deviation (MAD) values are a measure of precision of the component magnetization based on the geometry of the dataset and can be used to assess the quality of the directional data (Kirschvink, 1980). Intervals with MAD values higher than 10° are highlighted in Fig. 5. Only one of these intervals is found in the

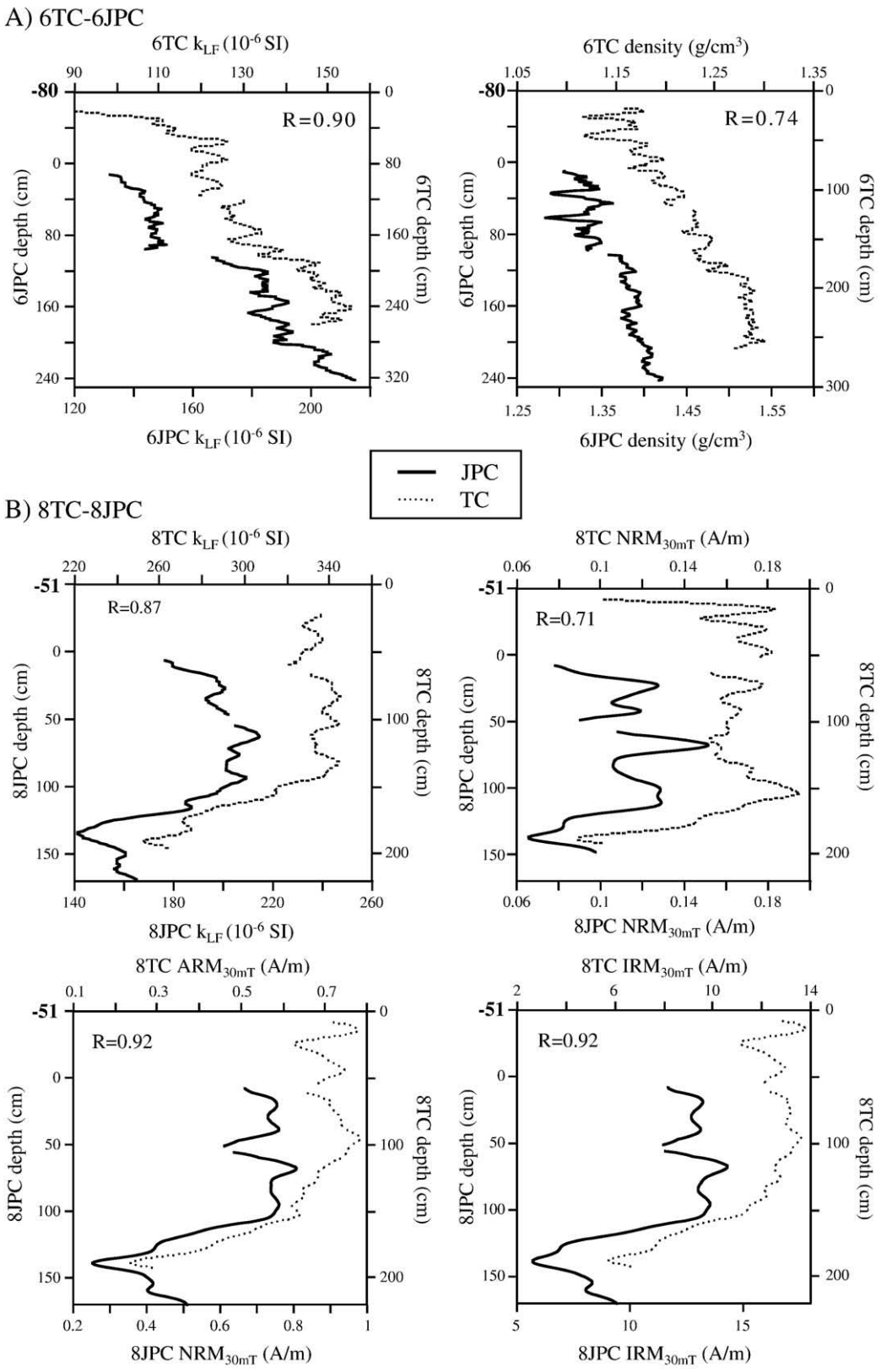

Fig. 2. Correlation of the physical and magnetic parameters between the jumbo piston core (JPC) and its trigger weight gravity core (TC) plotted with a 5 points moving average function for A) cores 6TC-6JPC and B) cores 8TC-8JPC. The magnetic susceptibility (k_{LF}) and bulk density measurements were acquired on board on whole cores, whereas the magnetic remanence values (NRM, ARM, IRM) were measured on u-channel samples. The linear correlation coefficient (R) is indicated for each graph. A key stratigraphic marker of cores 8JPC and 8TC is a minimum of all magnetic parameters (at ~130 cm and ~180 cm, respectively).

postglacial units, where MAD values are generally lower than 5° as recently proposed by Stoner and St-Onge (2007) for high quality Quaternary directional data. High MAD values generally reflect poorly defined ChRM due to incomplete filling of the u-channel (e.g., from 121 to 127 cm in the postglacial unit of core 6JPC, Fig. 5) or a magnetic mineral assemblage not suitable for recording the geomagnetic field,

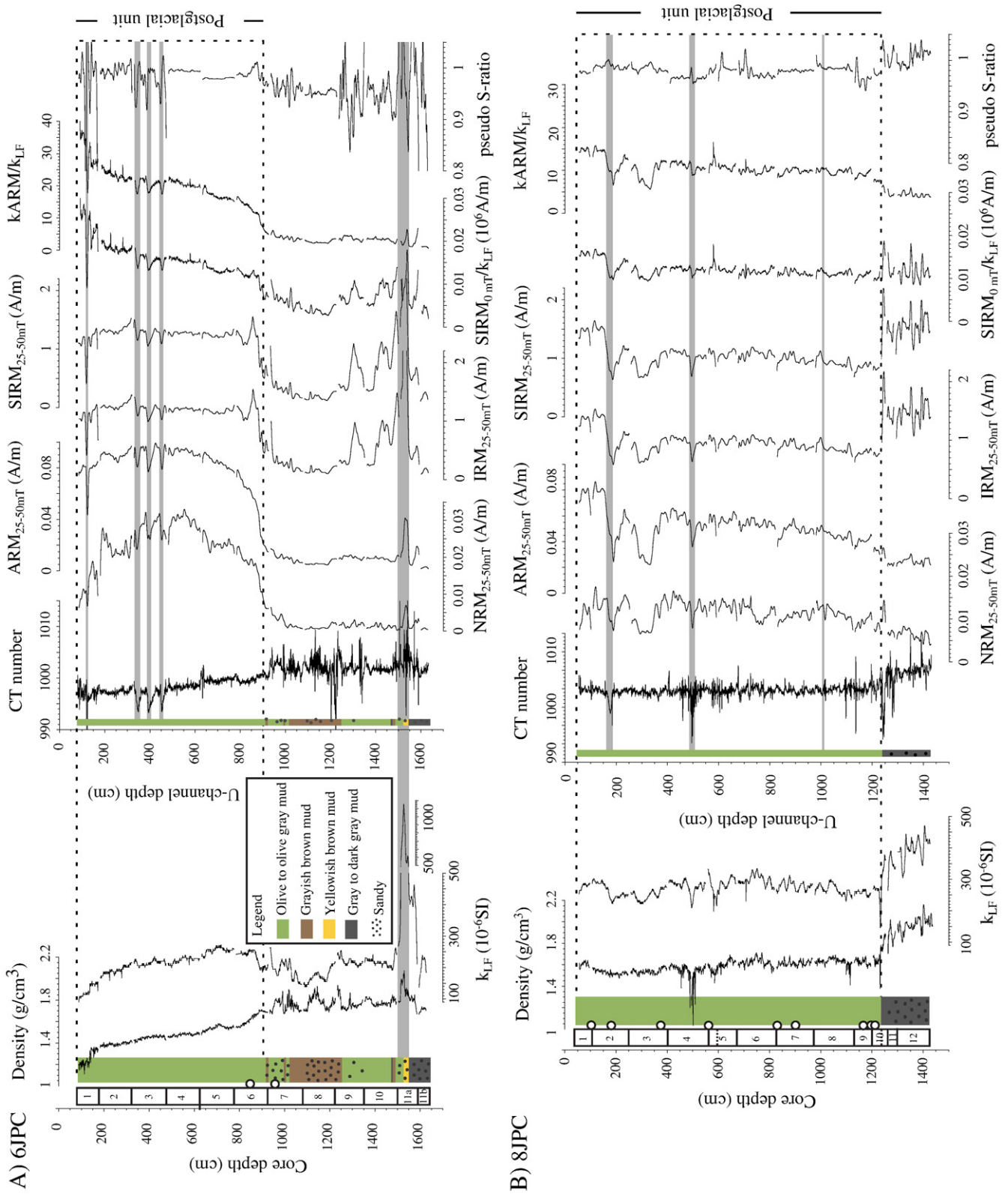

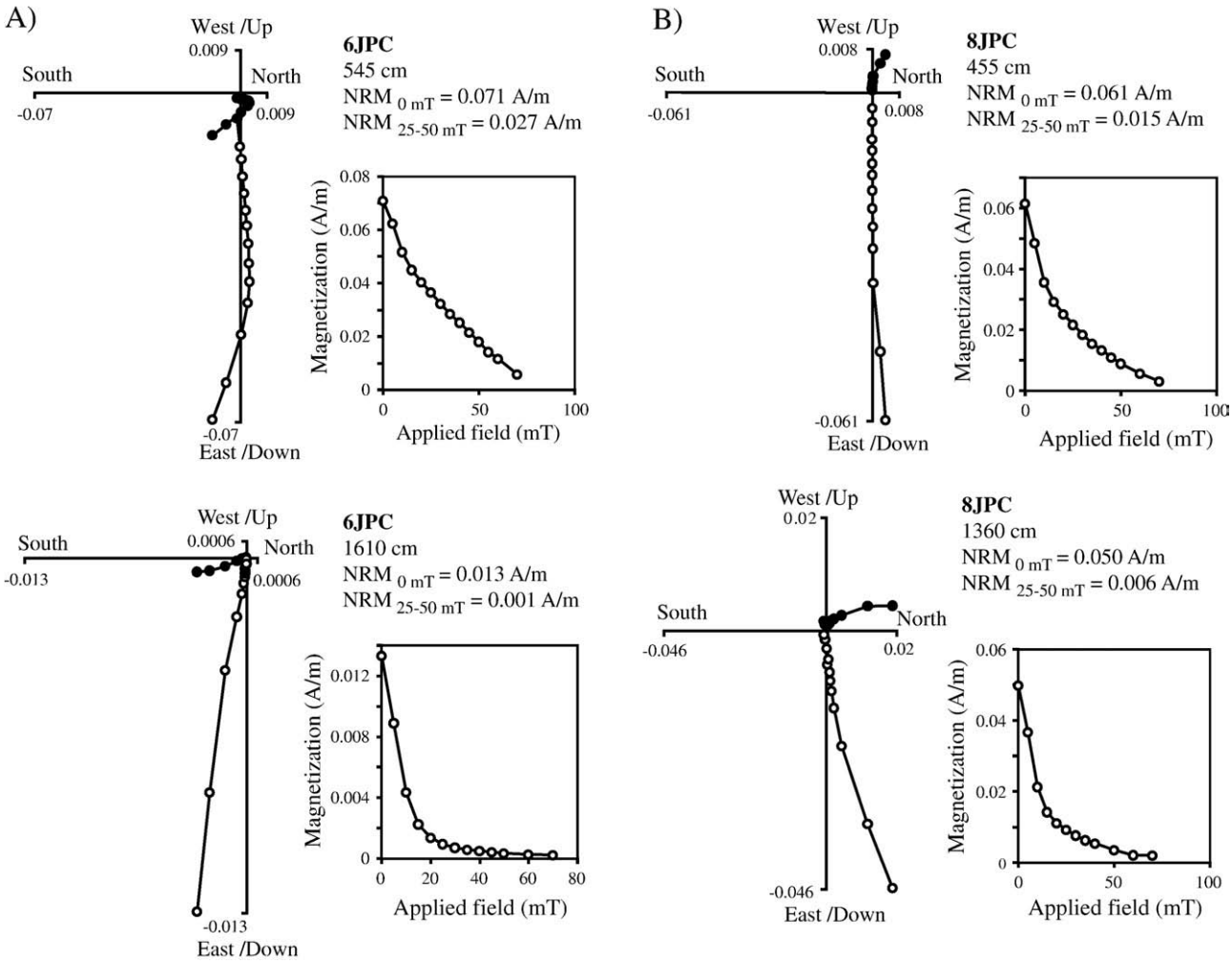

Fig. 4. AF demagnetization behavior and orthogonal projection diagrams of samples from the postglacial (top) and the basal (bottom) units of cores A) 6JPC and B) 8JPC. Open (close) circles denote projections on the vertical (horizontal) plane.

for example IRD-rich layers (e.g. highlighted intervals in both cores basal unit, Fig. 5).

4.4. Magnetic mineralogy

Pseudo S-ratio values are close to 1 (Fig. 3) with a postglacial mean of 0.99 and 0.98 for cores 6JPC and 8JPC, respectively. This indicates that saturation of the magnetic assemblage is achieved in a 0.3 T field, which is typical of low coercivity minerals such as magnetite. The shape of the hysteresis curves from both postglacial units (Fig. 6) is also characteristic of low coercivity ferrimagnetic mineral like magnetite (Tauxe et al., 1996), with saturation fields below 0.2 T. Furthermore, Mrs/Ms values ranging between 0.1 and 0.3 (Fig. 7) are typical of magnetite/titanomagnetite grains (Day et al., 1977; Tauxe, 1993). The pseudo S-ratio, the hysteresis curve and the Day plot suggest that the postglacial mineralogy is most likely dominated by magnetite. Thermomagnetic curves measured on nearby core 5JPC confirmed the presence of magnetite with Curie temperatures of 577–580 °C, and a second phase with Curie temperatures of 360–380 °C (Brachfeld et al., 2009-this issue). This lower Curie temperature was observed only in the heating curves, and was not reversible in experiments run from 25–350 °C only (Brachfeld et al., 2009-this issue). We speculate that this indicates the presence of greigite. However, the $IRM_{0\ mT}0.9\ T/k_{LF}$ postglacial averages of 15.8 kA/m and 12 kA/m for core 6JPC and 8JPC, respectively, verify that even though iron sulfides are present in the postglacial units, neither greigite nor pyrrhotite dominates the magnetic mineral assemblages (Maher et al., 1999). The average MDF for the postglacial sediments is 27.5 mT for core 6JPC and 12 mT for core 8JPC. These values are again consistent with magnetite and the presence of coarser grains in core 8JPC accounts for the lower MDFs (see Section 4.5).

Higher amplitude and frequency variations of the pseudo S-ratio in the basal units of both cores (Fig. 3) illustrate a varying magnetic mineralogy. The Day plot (Day et al., 1977) (Fig. 7) illustrates that samples from the basal unit of both cores generally fall in the lower part and outside the theoretical lines for PSD or multi-domain (MD) magnetite, suggesting a mineralogy that may not be entirely dominated by magnetite. The typical shape of the hysteresis curves of the basal units (Fig. 6) also indicates a higher paramagnetic contribution than in the

Fig. 3. Downcore physical and magnetic properties with simplified lithology of cores A) 6JPC and B) 8JPC. On the left panel: wet bulk density and magnetic susceptibility measured on the whole cores. On the right panel: computerized tomography (CT) number, remanent magnetizations ($NRM_{25–50\ mT}$, $ARM_{25–50\ mT}$, $IRM_{25–50\ mT}$ and $SIRM_{25–50\ mT}$), magnetic grain size indicators (k_{ARM}/k_{LF}, $SIRM_{0mT}/k_{LF}$) and magnetic mineralogy indicator (pseudo S-ratio) measured on u-channel samples. The upper dashed rectangle indicates the postglacial sedimentary unit of each core. Unreliable intervals are highlighted in gray (see text for details). Circles along the simplified lithologies represent the location of radiocarbon dated material as listed in Table 2. A schematic representation of each core with section breaks and section numbers is shown along the depth axes. The horizontal dashed line in Section 5 and 10 of core 8JPC represent additional section breaks for the u-channels only.

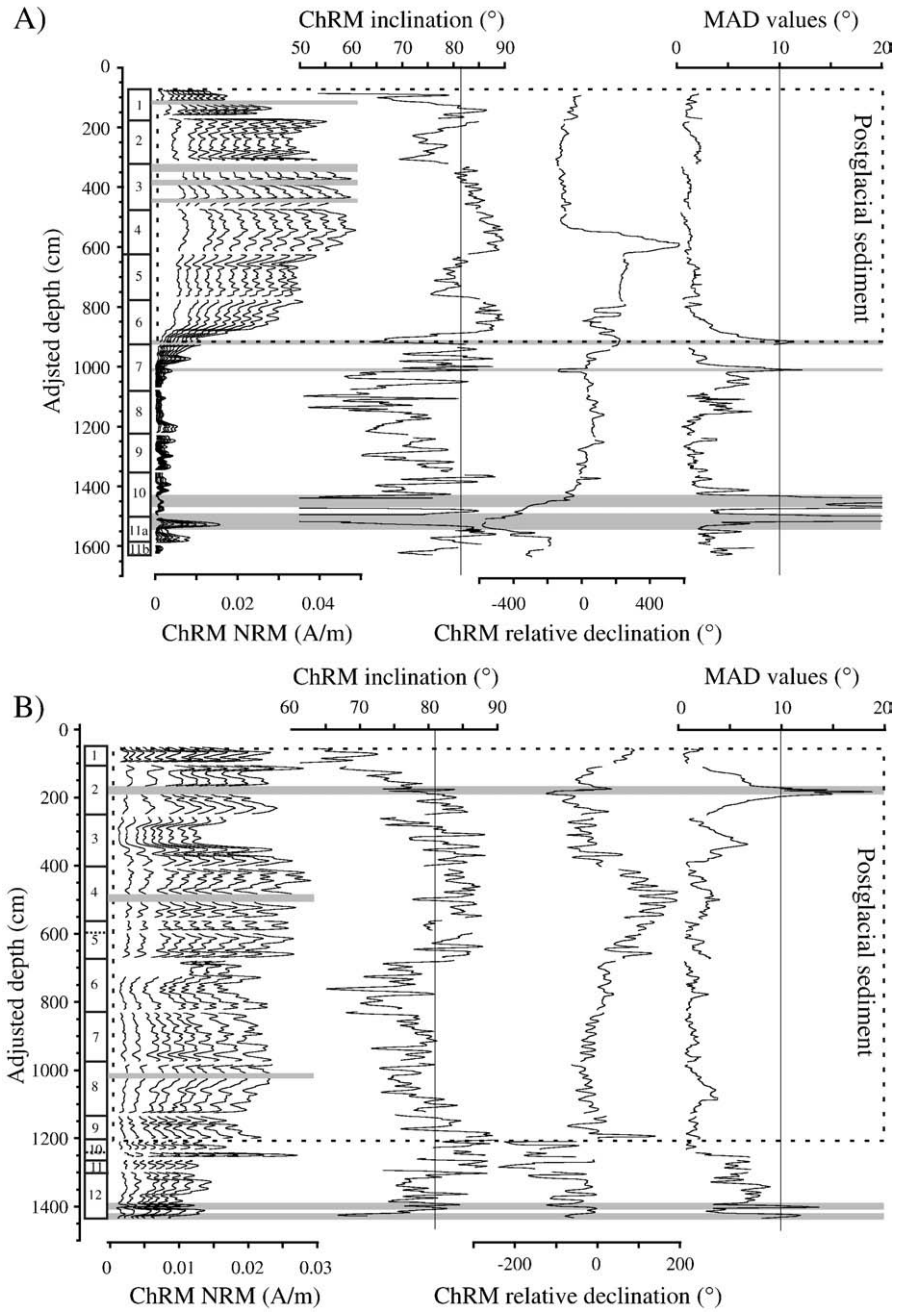

Fig. 5. Downcore variation of the NRM (demagnetization steps from 20 mT to 70 mT with 5 mT increments, right to left), ChRM inclination, declination and MAD values of cores A) 6JPC and B) 8JPC. The vertical line on the inclination graphs indicate the expected GAD value for the latitude of the sampling site. The dashed rectangle indicates the postglacial sedimentary unit of each core. Unreliable intervals are highlighted in gray (MAD values > 10° and/or disturbed sediment). A schematic representation of each core with section breaks and section numbers is shown along the depth axes, as in Fig. 3.

postglacial unit, in addition to the presence of higher-coercivity minerals such as (titano)hematite and goethite (Tauxe et al., 1996; Barletta et al., 2008; Brachfeld et al., 2009-this issue).

4.5. Magnetic grain size

The optimal magnetic grain size window for paleointensity determinations corresponds to magnetite grains from 1 to 15 μm characterized by pseudo-single domain (PSD) magnetic state (King et al., 1983; Tauxe, 1993). For the postglacial unit of cores 6JPC and 8JPC, the $IRM_{0\ mT}0.9$ T vs. k_{LF} diagram (Thompson and Oldfield, 1986) (Fig. 8) indicates magnetic grain sizes generally between 1 and 16 μm and the Day plot (Day et al., 1977) (Fig. 7) indicates a PSD magnetic grain size. The Day plot (Fig. 7) also suggests generally coarser PSD grains in core 8JPC than in core 6JPC. Similarly, the mean postglacial values of $IRM_{0\ mT}0.9$ T/k_{LF} and k_{ARM}/k_{LF} (Fig. 3) for core 8JPC (12 kA/m and 10.5, respectively) are lower than for core 6JPC (15.8 kA/m and 20, respectively) and indicate coarser mean magnetic grains in core 8JPC. The presence of slightly coarser grains in core 8JPC is not only attributed to magnetic grains. The average downcore mean grain size of the <45 μm fraction measured by laser diffraction is 14.2 ± 2.5 μm for core 8JPC and 7 ± 0.5 μm for core 5JPC (Darby et al., 2009-this issue), a core located approximately 25 km from core 6JPC on the continental slope (location in Fig. 1). Considered together, the magnetic grain size indicators suggest that the magnetic grain size of both core postglacial units is within or close to the theoretical PSD limits for magnetite and that core 8JPC contains coarser PSD grains than core 6JPC.

The postglacial unit of core 6JPC depicts a slight downcore increase of wet bulk density, k_{LF} and CT number with depth, while magnetic

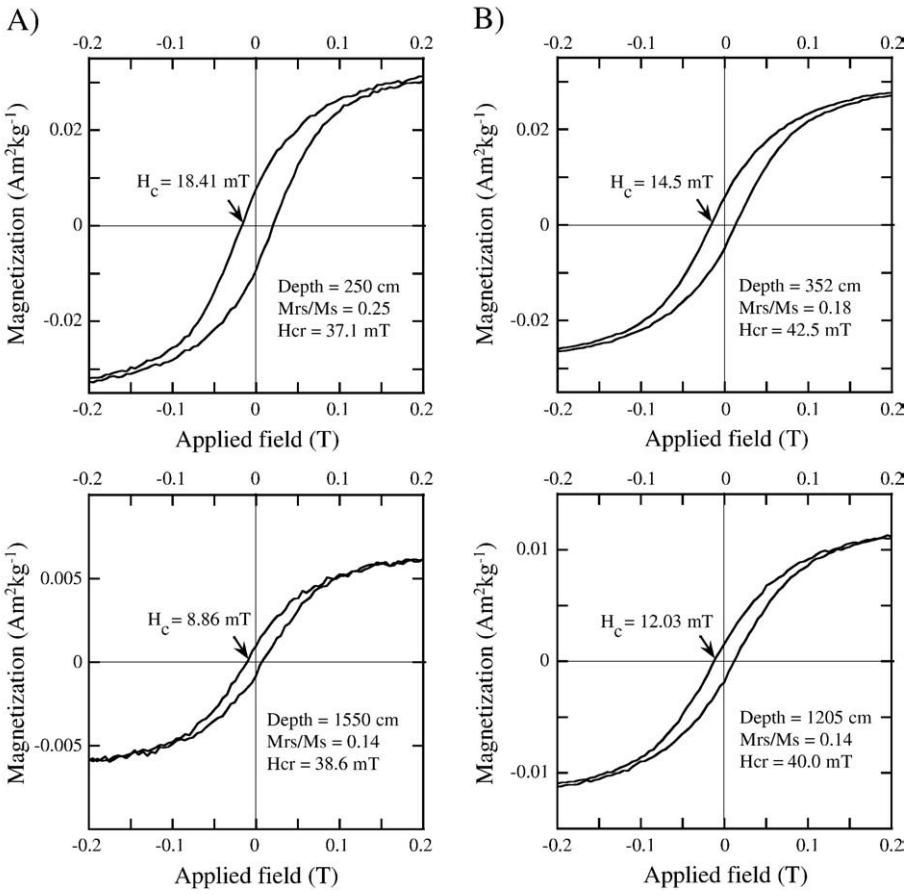

Fig. 6. Typical hysteresis curves and derived parameters for the postglacial unit (upper graph) and the basal unit (lower graph) of cores A) 6JPC and B) 8JPC. The coercivity of magnetic minerals (Hc), the coercivity of remanence (Hcr) and the ratio of the saturation remanence (Mrs) on the saturation magnetization (Ms) are indicated.

grain size indicators ($SIRM_{0\ mT}/k_{LF}$ and k_{ARM}/k_{LF}), $NRM_{25-50\ mT}$ and $ARM_{25-50\ mT}$ decrease (Fig. 3). These results suggest a trend of increasing magnetic grain size and/or a trend of decreasing concentration of the ferrimagnetic material with depth. Such a long-term trend was also observed in core HLY-0501-05JPC (Barletta et al., 2008), but is absent in core 8JPC. Finally, in the basal unit of both cores, the magnetic grain size ratios ($SIRM_{0\ mT}/k_{LF}$ and k_{ARM}/k_{LF}) as well as the Day plot (Figs. 3 and 7) indicate the occurrence of coarser grains.

4.6. Magnetic concentration

Rock magnetic parameters all depend on the concentration of magnetic materials present in a sediment sample. Therefore, the optimal sediment sequence for relative paleointensity determinations has a uniform concentration of magnetic grains. Despite the possible decrease in magnetic grains concentration with depth in core 6JPC (see Section 4.5) and an interval of low k_{LF} in the uppermost 179 cm of core 6JPC (background dataset), concentration variations of both sedimentary records stand below a factor of 10. This degree of variability is satisfying for paleointensity reconstructions (Tauxe, 1993).

5. Discussion

5.1. Initial stratigraphy

The physical and magnetic properties of cores 6JPC and 8JPC lead to the identification of two major sedimentary units: an upper postglacial unit and a bottom glacial/deglacial unit (Fig. 3). The basal units display higher amplitude and higher frequency changes of the magnetic mineralogy, as well as coarser magnetic grain sizes and intervals with MAD values >10° (Fig. 5). Because of this heterogeneity, we will now focus on the postglacial units.

The postglacial units have a homogeneous lithology and most likely contain sediment eroded from the previously glaciated North American continent. Such terrains are generally an excellent source of

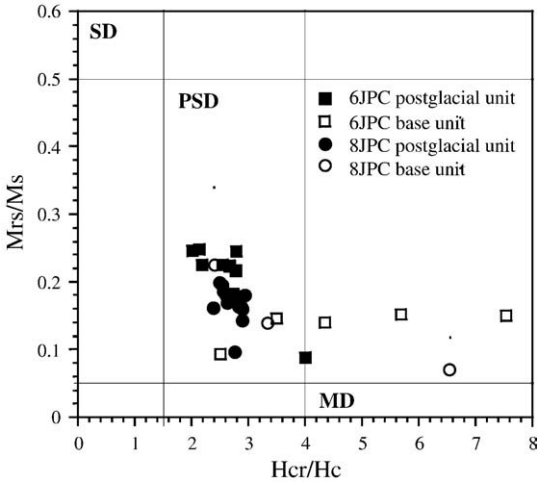

Fig. 7. Day plot (Day et al., 1977) of cores 6JPC and 8JPC pilot samples. All samples from the postglacial units (solid symbols) fall in the pseudo-single domain (PSD) range for magnetite.

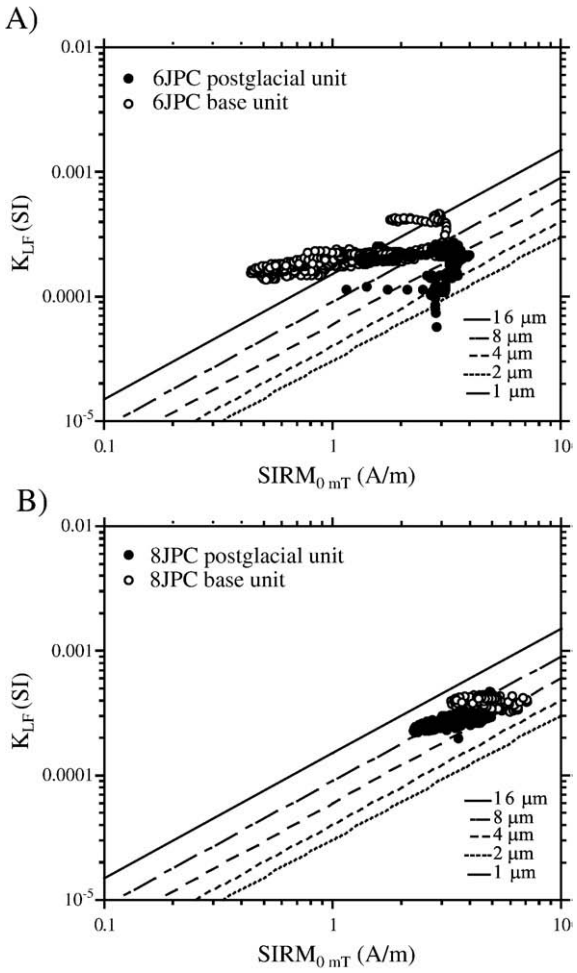

Fig. 8. Estimation of magnetic grain size for cores A) 6JPC and B) 8JPC. The reference lines for magnetite are from Thompson and Oldfield (1986).

fine-grained magnetic minerals for geomagnetic recording (Stoner and St-Onge, 2007). In fact, an abundance of silt- and sand-size magnetic minerals, particularly magnetite and titanomagnetite occur in sediments along the Alaskan margin and throughout the Arctic Ocean (Darby, 2003; Darby and Bischof, 2004; Bischof and Darby, 1997, 1999).

5.2. Preliminary age model

The radiocarbon-based age model of core 8JPC is presented in Fig. 9. A sharp and unlikely inversion in sedimentation rates would be assumed at the base of the postglacial unit if all dates were considered. Therefore the only date derived from a gastropod shell was considered too old (remobilized) and excluded (core 8JPC at 1201 cm; Table 2).The remaining ages were derived from 8 bivalve shells well distributed on the 12 m of postglacial sediment with a mean distance of 157+/−99 cm. This age model is consistent with the very high sedimentation rates (>100 cm/kyr) observed on the western Arctic margin during the early Holocene (Hill et al., 1991; Keigwin et al., 2006; Barletta et al., 2008). As a result, the resolution of paleomagnetic measurements on core 8JPC is very high, especially between 5000 and 8000 cal BP, where the average estimated sedimentation rate is 348 cm/kyr. The age model of core 8JPC suggests a major decrease of sediment supply (approximately 9 times less; Fig. 9) on the continental shelf near Barrow Canyon beginning around 5000 cal BP. Similar steep changes in sedimentation rates have been observed on the continental shelf of the Laptev Sea (Bauch et al., 2001), in Hope Valley (west of Alaska) and on the upper Chukchi slope near Barrow canyon (Keigwin et al., 2006), whereas it is not observed on the lower Alaskan slope (Barletta et al., 2008). This change in sedimentation rate on Western Arctic continental shelves might be linked to the stabilization of sea level after the last marine transgression, in conjunction with the intensification of currents near Barrow Canyon (Darby et al., 2009-this issue).

5.3. Record reliability for relative paleointensity determination

The results presented above indicate that cores 6JPC and 8JPC postglacial units satisfy the criteria for the determination of paleomagnetic secular variation (PSV) and relative paleointensity (RPI) records (e.g., King et al., 1983; Tauxe, 1993; Stoner and St-Onge, 2007). These criteria include the following:

1) There is a strong and stable well-defined single component characteristic remanent magnetization (ChRM; Fig. 4);
2) MAD values are generally lower than 5° and ChRM inclinations vary around the theoretical GAD inclination for each site (Fig. 5);
3) The magnetic remanence carrier is PSD magnetite (Figs. 7, 8);
4) Changes in the magnetic concentration vary by less than 1 order of magnitude (background dataset).

5.4. Relative paleointensity proxy

The NRM recorded by sediments reflects changes in both the geomagnetic field intensity and the concentration of ferrimagnetic material (e.g., Tauxe, 1993). To compensate for the effect of concentration changes on the measured NRM and to obtain a relative paleointensity record, the NRM is commonly normalized by a

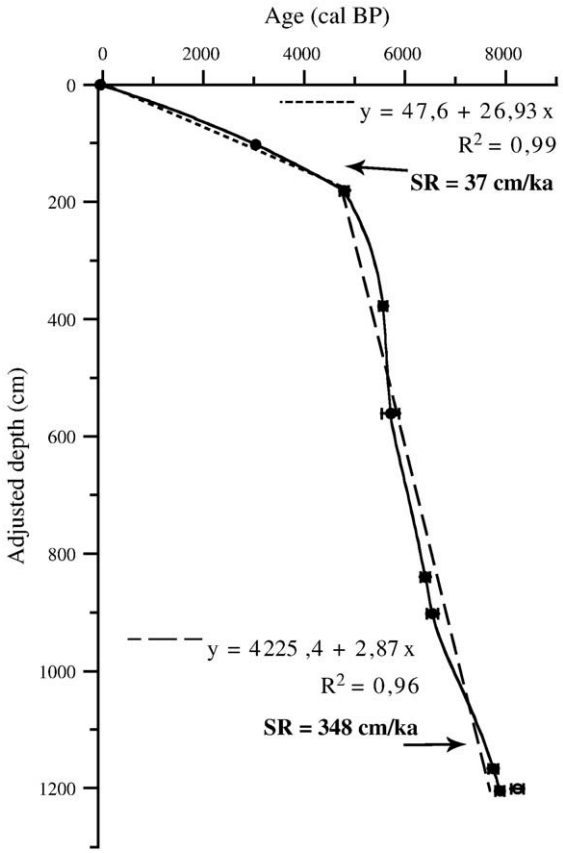

Fig. 9. Radiocarbon-based age model of core 8JPC. Linear fit (dashed lines) equations and estimated sedimentation rates (SR) are indicated. The excluded date is shown with an open symbol.

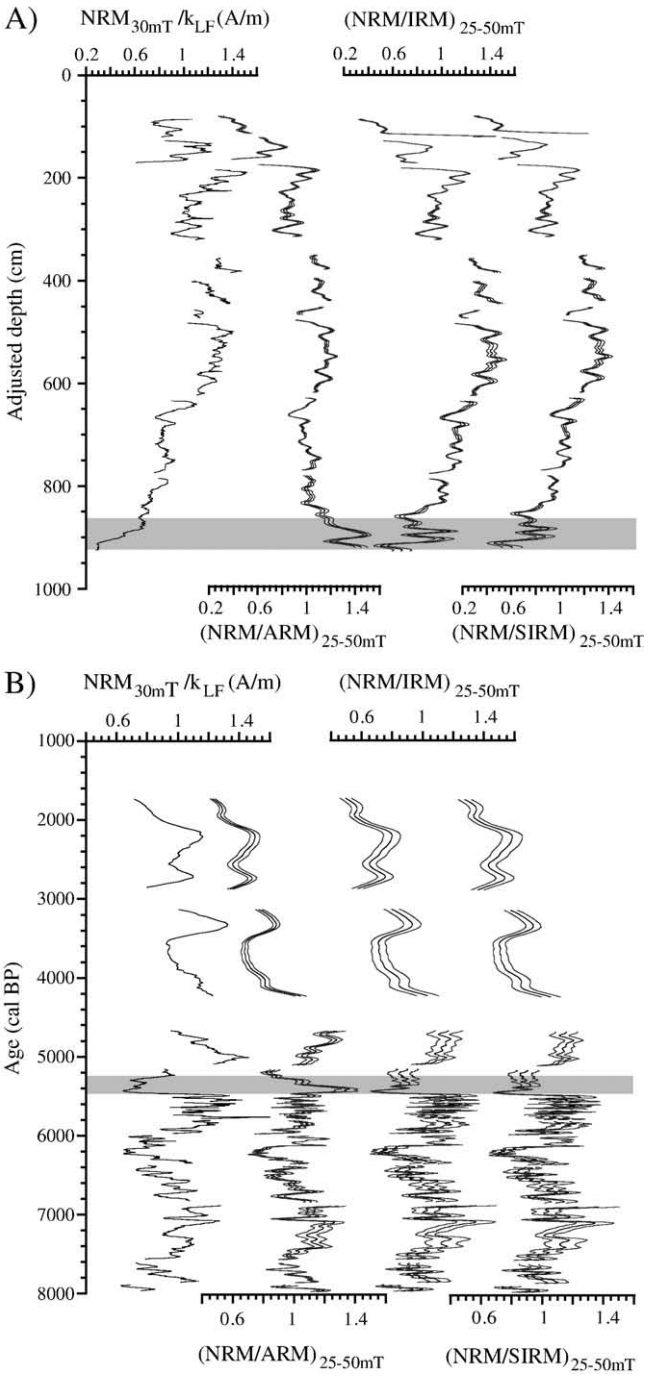

Fig. 10. Normalized intensity ($NRM_{30\ mT}/k_{LF}$, $(NRM/ARM)_{25–50\ mT}$, $(NRM/IRM)_{25–50\ mT}$, $(NRM/SIRM)_{25–50\ mT}$) for cores A) 6JPC and B) 8JPC. The standard deviation for each ratio mean is represented by double gray lines. Gray intervals highlight where the four normalization parameters results in different relative paleointensity behavior.

concentration-dependant rock magnetic parameter (e.g., NRM/k_{LF}, NRM/ARM, NRM/IRM, NRM/SIRM; e.g., see reviews of Tauxe, 1993; Valet, 2003; Stoner and St-Onge, 2007).

The average over the demagnetization steps 25 to 50 mT (6 steps) was used for NRM/ARM, NRM/IRM and NRM/SIRM, as these steps are part of the ChRM and each individual ratio is consistent over this interval (small standard deviations, Fig. 10). All normalized intensity records ($NRM_{30\ mT}/k_{LF}$, $(NRM/ARM)_{25–50\ mT}$, $(NRM/IRM)_{25–50\ mT}$ and $(NRM/SIRM)_{25–50\ mT}$) were divided by their mean value for inter-comparison. The four ratios yield similar profiles (Fig. 10), except for one interval in each core (gray intervals in Fig. 10), where low ARM values have been observed (Fig. 3 and square symbols in background dataset). Apart from these two intervals, the overall similarity of the normalized magnetic remanence records for each core suggests that the same magnetic assemblages are activated. The $NRM_{30\ mT}/k_{LF}$, $(NRM/IRM)_{25–50\ mT}$ and $(NRM/SIRM)_{25–50\ mT}$ of both cores are not correlated with their normalizer ($R^2<0.1$), whereas $(NRM/ARM)_{25–50\ mT}$ for core 8JPC seems slightly correlated ($R^2=0.1$ for core 6JPC and 0.4 for core 8JPC).

Cross-spectral analysis reveals that the relative paleointensity proxies of core 6JPC are not coherent with their normalizers, whereas $NRM_{30\ mT}/k_{LF}$ and $(NRM/ARM)_{25–50\ mT}$ of core 8JPC appear coherent at the 95% confidence level over several frequencies (Fig. 11). $(NRM/IRM)_{25–50\ mT}$ is the least coherent (Fig. 11B), with a significant peak only observed at a period centered around 120 years. Because a paleointensity estimate should not correlate with bulk rock magnetic parameters (Tauxe, 1993), $(NRM/IRM)_{25–50\ mT}$ is the chosen ratio for cores 6JPC and 8JPC.

5.5. Paleomagnetic secular variation and relative paleointensity records in the Western Arctic

In order to assess the quality of the paleomagnetic records of core 6JPC and 8JPC on a regional scale and to constrain the chronology of core 6JPC, which has only one radiocarbon date in the postglacial unit, the paleomagnetic vectors (inclination, declination and relative paleointensity records) were compared together, as well as with a recently published nearby record (core 5JPC; Barletta et al., 2008; location in Fig. 1). The full vector correlation of the three cores from the Alaskan margin is supported by the available Holocene records from the Beaufort

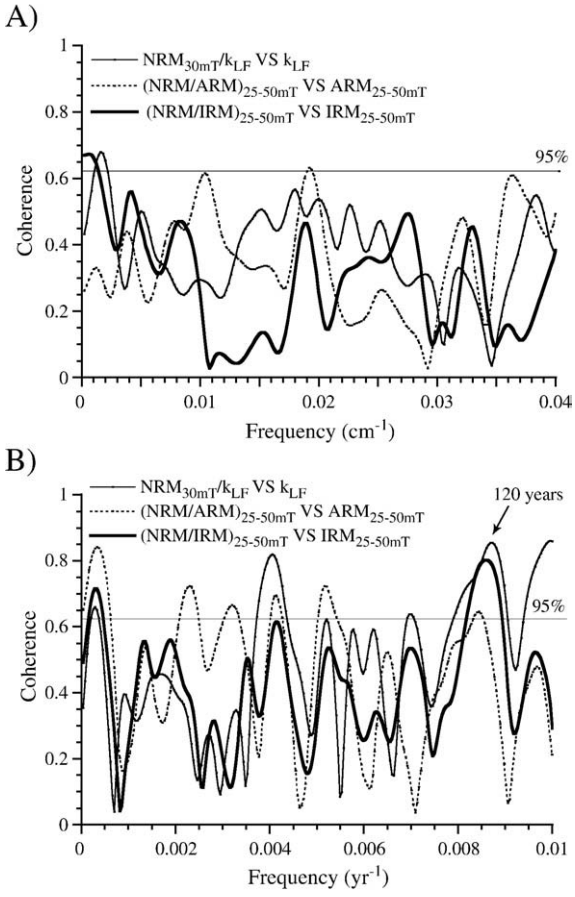

Fig. 11. Coherence of the relative paleointensity proxies with their normalizers for cores A) 6JPC and B) 8JPC. The horizontal line represents the 95% confidence level. A Blackman–Tuckey cross-spectral analysis using a Barlett window (Paillard et al., 1996) was applied. $(NRM/SIRM)_{25–50\ mT}$ vs. $SIRM_{25–50\ mT}$ (not shown) is similar to $(NRM/IRM)_{25–50\ mT}$ vs. $IRM_{25–50\ mT}$.

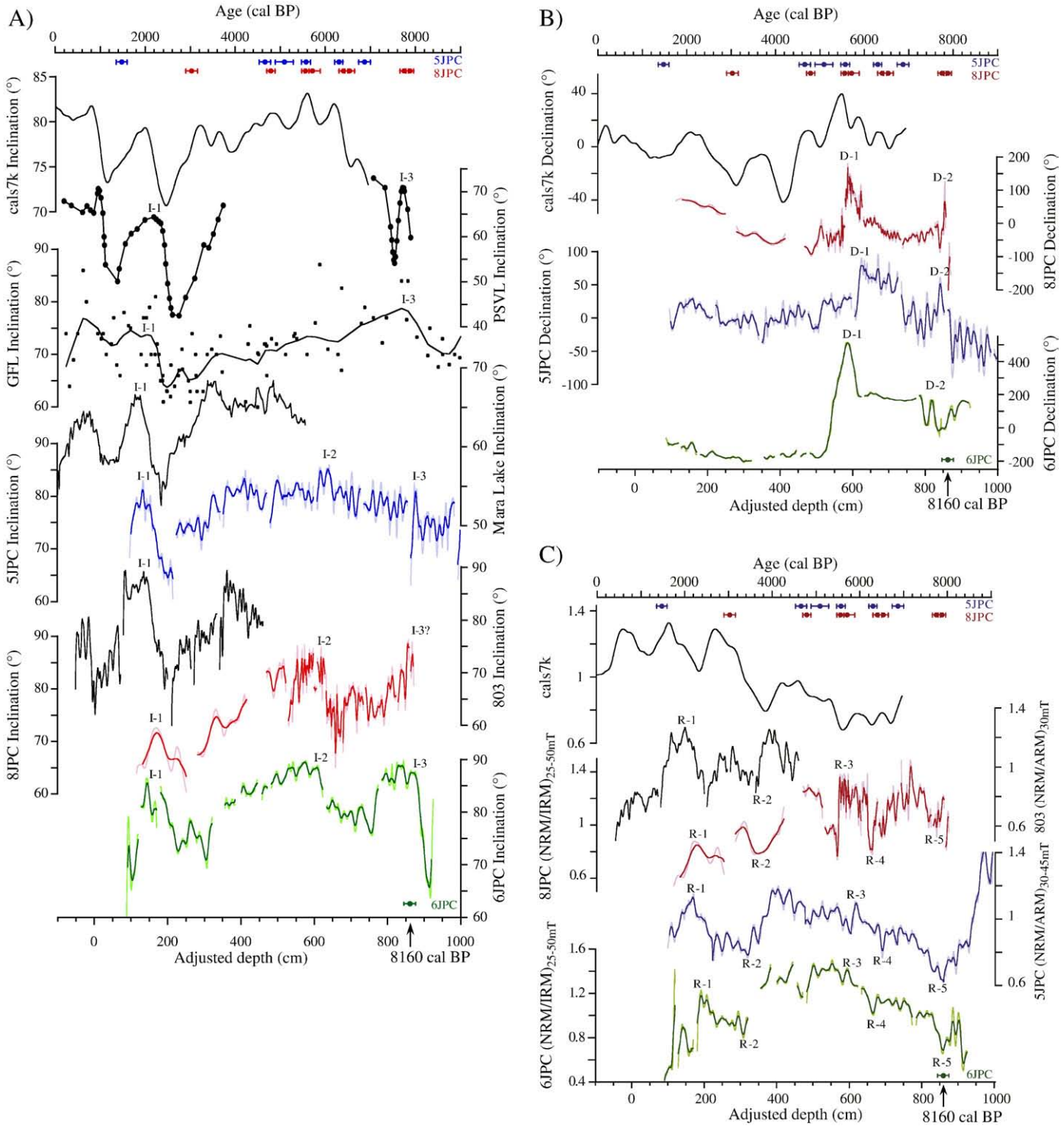

Fig. 12. Full vector paleomagnetic comparison of cores 6JPC and 8JPC with regional records on their own chronology. Core 6JPC is shown with its adjusted depth scale. A) Inclination, B) declination and C) relative paleointensity records from Western North American volcanic rocks (PSVL; Hagstrum and Champion, 2002), Grandfather Lake sediments, Alaska (GFL; Geiss and Banerjee, 2003), Beaufort Sea and Alaskan margin sediments (cores 803 and 5JPC; Barletta et al., 2008), Mara Lake sediments, Western Canada (MR; Turner, 1987). Also illustrated are the cals7k spherical harmonic outputs for the Alaskan margin (71.63°N, 156.87°W; derived from Korte and Constable, 2005). The Mara Lake chronology was calibrated using the IntCal04 calibration curve (Reimer et al., 2004). The pale line on the Alaskan margin plots (5JPC, 6JPC and 8JPC) represents the high-resolution records and the dark line represents an 11 points moving average function. Correlative features discussed in the text and listed in Table 3 are illustrated. The radiocarbon dates from cores 5JPC and 8JPC are indicated with error bars along the age scale and the available radiocarbon date for core 6JPC is indicated on the adjusted depth scale.

Sea (core 803; Barletta et al., 2008) and from high latitude sites in Western North America from British Columbia, Canada (Mara Lake (ML); Turner, 1987) to Alaska, USA (Grandfather Lake (GFL); Geiss and Banerjee, 2003). Cores 5JPC, 803 and Grandfather Lake have a radiocarbon-based chronology, whereas the chronology of Mara Lake is based on the age of the Mt St Helens tephra. For comparison to paleomagnetic secular variation records that are not affected by radiocarbon reservoir effect nor complicated by old carbon issues, we also compare cores 6JPC and 8JPC with the Holocene Western USA compilation from lava flows (PSVL; Hagstrum and Champion, 2002). Comparison of these records

Table 3
Ages of paleomagnetic inclination, declination and paleointensity features used for the identification of tie points.

Paleomagnetic feature	6JPC adjusted depth (cm)		Age (cal BP)						Mean age (cal BP)	Standard deviation (yr)
	80 cm offset	147 cm offset	5JPC	8JPC	803	GFL	ML	PSVL		
I-1	144	211	1900	2200	2000	2100	1850	2150	2030	130
R-1	192	259	2200	2250	2000				2150	110
R-2	308	375	3450	3650	3650				3580	90
D-1	586	653	5900	5650					5780	130
R-3	595	662	5850	5500					5680	180
I-2	607	674	6050	5950					6000	70
R-4	666	733	6450	6200					6330	130
D-2	819	886	7750	7850					7800	50
R-5	859	926	7650	7700					7680	30
I-3	882	949	8000			7800		7700	7830	120

(Fig. 12) reveals the overall agreement between the three HOTRAX records (5JPC, 6JPC and 8JPC) and with other high latitude Western North American records, indicating that cores 6JPC and 8JPC have recorded coherent changes in Earth's magnetic field behavior. There are numerous correlative features, including abrupt ones (e.g., I-1, D-1; Fig. 12A and B) where rapid directional changes have been recorded. The geomagnetic inclination, declination and paleointensity records calculated for the coring sites (position of core 8JPC; Table 1) using the cals7k spherical harmonic model (Korte and Constable, 2005; Fig. 12A, B and C) are also shown and depict similar PSV and paleointensity profiles at the millennial to centennial timescale. This similarity supports both the reliability of the Western Arctic records and the overall validity of directional and paleointensity data of the model cals7k even though no Arctic dataset was used to constrain the model.

The feature I-1 at an estimated mean age of 2030 +/− 130 cal BP (Table 3) is particularly striking (Fig. 12A) and is characterized by a large amplitude change in all available Western North American records. In addition, all paleomagnetic inclination records (Fig. 12A) yield the same general shallowing trend from ~6000 to 2500 cal BP, followed by a sharp inclination steepening (ending at feature I-1). The three Alaskan margin records (5JPC, 6JPC and 8JPC) present a major declination swing beginning at 5660 ± 160 cal BP and ending at feature D-1 (Fig. 12B; Table 3), with amplitudes of 700°, 250° and 95°, and for duration of 70 cm, 160 and 130 years for cores 6JPC, 8JPC and 5JPC, respectively. The declination feature D-1 is not located at section breaks and the difference in amplitude could have resulted from different rates of core twisting during piston coring. The relative paleointensity estimates of cores 5JPC and 6JPC are very similar and

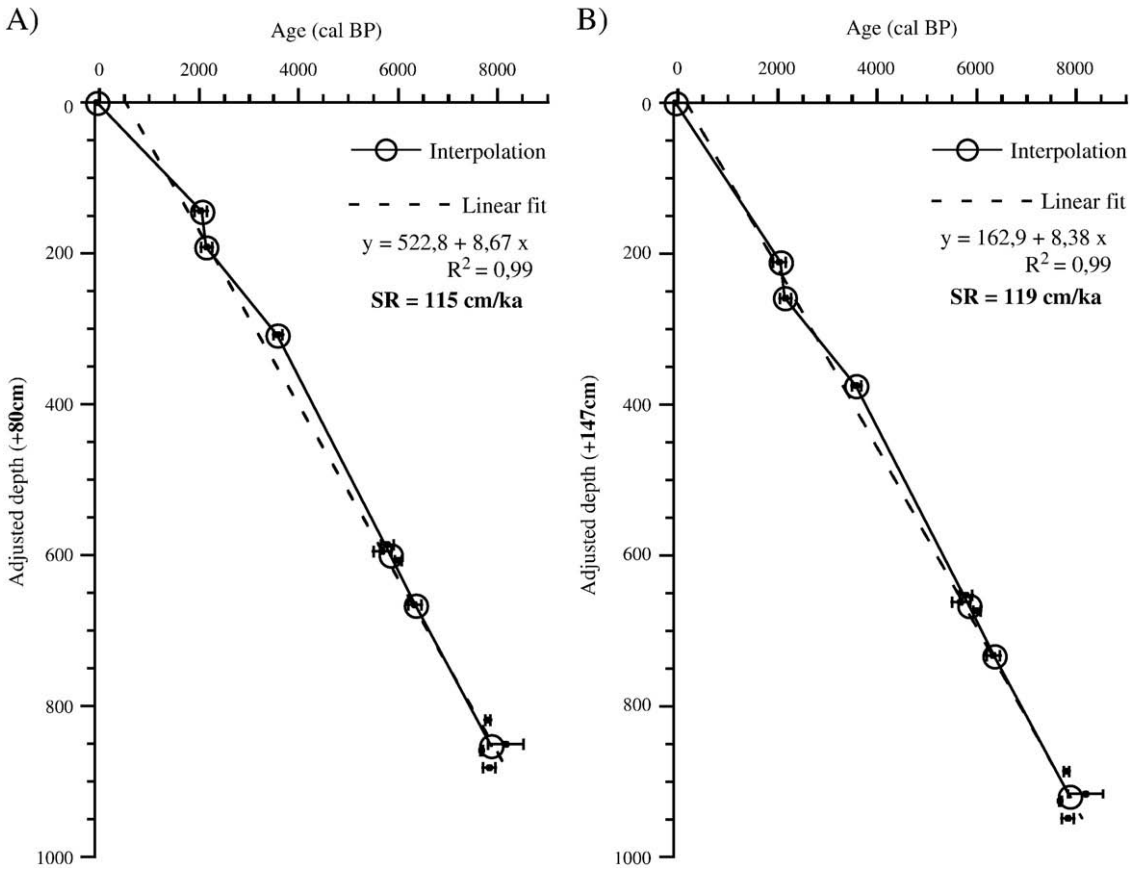

Fig. 13. Depth vs. age diagram of core 6JPC based on the identified paleomagnetic tie points (Table 3) considering an offset of A) 80 cm and B) 147 cm between the piston (6JPC) and the trigger weight (6TC) cores. Both age models fall within the error bar limits of the available radiocarbon date (Table 2) shown with a thicker symbol. The black line is an interpolation between points or cluster of points (Ortiz et al., 2009-this issue) and the dashed line represents a linear fit in all the points. The linear fit equation and derived sedimentation rate (SR) for the two possible adjusted depth-scales of core 6JPC (dashed line) are illustrated for comparison.

allowed the identification of 5 tie points also observed in cores 8JPC and 803 (Fig. 12C).

A total of 10 correlation tie points (Fig. 12 and Table 3) have been used to constrain the chronology of core 6JPC. The standard deviation for a given feature was at most 180 years. This difference is likely associated with radiocarbon dating and radiocarbon reservoir effect uncertainties. The ages of the comparison-based tie points for the postglacial unit of core 6JPC (Fig. 13) are consistent with the available radiocarbon date obtained at 850–852 cm (Table 2) and, assuming a linear sedimentation rate, are comparable to the age model of core 5JPC (Barletta et al., 2008), which was cored nearby on the slope (Fig. 1). The two plausible offsets between core 6JPC and its trigger core do not affect the estimated sedimentation rate for the postglacial unit (Fig. 13) or the ages of the paleomagnetic features (Table 3). Moreover, the coincidence of paleomagnetic features between the spherical harmonic model prediction and the lava flow compilation, which are not affected by reservoir effects, along with the marine and lacustrine sedimentary records from Western North America (Fig. 12) supports the use of a ΔR of 0 at the Alaskan margin.

The difference in postglacial sediment thickness found at the two sites (6JPC and 8JPC; Figs. 1 and 3) suggests higher sedimentation rates at core site 8JPC than at 6JPC, notably between 5000 and 8000 cal BP. The estimated sedimentation rate during this interval for core 8JPC is 348 cm/kyr (Fig. 9), while the Holocene sediment of cores 6JPC and 5JPC would have accumulated at about 115 cm/kyr (Fig. 13A) and 144 cm/kyr (Barletta et al., 2008), respectively. Since core 8JPC is located near the Barrow Canyon on the continental shelf, overflow deposits as well as the proximity to the coast may account for the sediment supply difference. The proximity of Barrow Canyon could also explain the presence of coarser PSD magnetic grains in core 8JPC than in core 6JPC (Figs. 7, 8), as core 6JPC was from the lower mid-slope in deeper waters and further away from the sediment source than core 8JPC. Despite their proximity to each other, cores 8JPC and 6JPC have considerably different sedimentation histories as core 8JPC is located on the continental shelf near the Barrow Canyon and is strongly controlled by changes in sea level and changes in hydrodynamic conditions.

6. Conclusions

Cores 6JPC and 8JPC represent two new high-resolution full vector paleomagnetic archives covering the postglacial period in the Western Arctic. The chronology of core 8JPC is radiocarbon-based and the chronology of core 6JPC is based on ten paleomagnetic tie points and one radiocarbon date. Full paleomagnetic vector comparison (inclination, declination and relative paleointensity) was used to constrain the chronology of core 6JPC using three nearby high-resolution marine sedimentary sequences and other Western North American records including high latitude lacustrine sequences and a compilation of lava flows. Consistent centennial- to millennial-scale inclination, declination and relative paleointensity features are identified in the marine Western Arctic records (5JPC, 6JPC, 8JPC and 803), allowing their use as regional chronostratigraphic markers. Since dating marine sediment is not straightforward at high latitudes, this study thus highlights the usefulness of high-resolution paleomagnetic records for the development of high-resolution Holocene Arctic chronostratigraphies.

Acknowledgements

We are grateful to the captain, officers, crew and scientists on board the USCGC Healy during the HOTRAX 2005 expedition funded by the United States National Science Foundation (US NSF) grant OPP-0352395 to D. Darby. We thank Joe Ortiz and Leonid Polyak for fruitful discussions on the stratigraphy of the HOTRAX cores, as well as C.E. Geiss and M. Korte for sharing their paleomagnetic data. We also thank André Rochon, Laurie Brown and two anonymous reviewers for constructive comments on the manuscript. This study was supported by the Natural Sciences and Engineering Research Council of Canada (IPY Special opportunity and Discovery grants) and the Polar Climate Stability Network. We also acknowledge the financial support of the Canadian Foundation for Innovation for the acquisition and operation of the cryogenic magnetometer and US NSF grant OPP-0612365 to S. Brachfeld. This is GEOTOP research center contribution no. 2009-0008.

Appendix A. Supplementary data

Supplementary data associated with this article can be found, in the online version, at doi:10.1016/j.gloplacha.2009.03.015.

References

Andrews, J.T., Jennings, A.E., 1990. Geomagnetic secular variations (inclination) of high latitude fiord cores: eastern Canadian Arctic. Polar Research 8, 245–259.
Andrews, J.T., Mothersill, J.S., Tabrez, A.R., 1986. Paleomagnetic record, texture, and mineralogy of Late Quaternary sediments, Baffin Island Fjords, N.W.T, Canada. Arctic and Alpine Research 18 (4), 361–376.
Barletta, F., St-Onge, G., Channel, J.E.T., Darby, D.A., 2008. High resolution paleomagnetic secular variation and relative paleointensity records from the western Canadian Arctic: implication for Holocene stratigraphy and geomagnetic field behavior. Submitted to Canadian journal of Earth Sciences 45, 1265–1281.
Bauch, H.A., Mueller-Lupp, T., Taldenkova, E., Spielhagen, R.F., Kassens, H., Grootes, P.M., Thiede, J., Heinemeier, J., Petryashov, V.V., 2001. Chronology of the Holocene transgression at the North Siberian margin. Global and Planetary Change 31, 125–139.
Bischof, J.A., Darby, D.A., 1997. Mid to Late Pleistocene ice drift in the western Arctic Ocean: evidence for a different circulation in the past. Science 277, 74–78.
Bischof, J.A., Darby, D.A., 1999. Quaternary ice transport in the Canadian Arctic and extent of Late Wisconsinian glaciations in the Queen Elizabeth Islands. Canadian Journal of Earth Sciences 36, 2007–2022.
Brachfeld, S., Banerjee, S.K., 2000. A new high-resolution geomagnetic relative paleointensity record for the North American Holocene: a comparison of sedimentary and absolute intensity data. Journal of Geophysical Research 105, 821–834.
Brachfeld, S., Barletta, F., St-Onge, G., Darby, D., Ortiz, J., 2009. Impact of diagenesis on the environmental magnetic record from a Holocene sedimentary sequence from the Chukchi-Alaskan margin, Arctic Ocean. Global and Planetary Change 68, 100–114 (this issue).
Creer, K.M., Tucholka, P., 1982. Construction of type curves of geomagnetic secular variation for dating lake sediments from east central North America. Canadian Journal of Earth Sciences 19, 1106–1115.
Dankers, P., 1981. Relationship between median destructive field and remanent coercive forces for dispersed natural magnetite, titanomagnetite and hematite. Geophysical Journal of the Royal Astronomical Society 64, 447–461.
Darby, D.A., 2003. Sources of sediment found in sea ice from the western Arctic Ocean, new insights into processes of entrainment and drift patterns. Journal of Geophysical Research 108, 13–1:13-10.
Darby, D.A., Bischof, J.F., 2004. A Holocene record of changing Arctic Ocean ice drift analogous to the effects of the Arctic Oscillation. Paleoceanography 19, PA1027.
Darby, D.A., Bischof, J., Jones, G.A., 1997. Radiocarbon chronology of depositional regimes in the western Arctic Ocean. Deep-Sea Research II 44, 1745–1757.
Darby, D.A., Polyak, L., Bauch, H.A., 2006. Past glacial and interglacial conditions in the Arctic Ocean and marginal seas — a review. Progress in Oceanography 71, 129–144.
Darby, D.A., Ortiz, J., Polyak, L., Lund, S., Jakobsson, M., Woodgate, R.A., 2009. The role of currents and sea ice in both slowly deposited central Arctic and rapidly deposited Chukchi-Alaskan margin sediments. Global and Planetary Change 68, 58–72 (this issue).
Day, R., Fuller, M., Schmidt, V.A., 1977. Hysteresis properties of titano-magnetite: grain-size and compositional dependence. Physics of the Earth and Planetary Interiors 13, 260–267.
Frank, U., Nowaczyk, N.R., Negendank, J.F.W., Melles, M., 2002. A paleomagnetic record from lake Lama, northern Central Siberia. Physics of the Earth and Planetary Interiors 133, 3–20.
Geiss, C.E., Banerjee, S.K., 2003. A Holocene–Late Pleistocene geomagnetic inclination record from Grandfather lake, SW Alaska. Geophysical Journal International 153, 497–507.
Gogorza, C.S.G., Sinito, A.M., Vilas, J.F., Creer, K.M., Nuñez, H., 2000. Geomagnetic secular variations over the last 6500 years as recorded by sediments from the lakes of south Argentina. Geophysical Journal International 143, 787–798.
Gogorza, C.S.G., Lirio, J.M., Nuñez, H., Chaparro, M., Bertorello, H.R., Sinito, A.M., 2004. Paleointensity studies on Holocene–Pleistocene sediments from lake Escondito, Argentina. Physics of the Earth and Planetary Interiors 145, 219–238.
Guyodo, Y., Valet, J.-P., 1996. Relative variations in geomagnetic intensity from sedimentary records: the past 200,000 years. Earth and Planetary Science Letters 143, 23–36.
Guyodo, Y., Valet, J.-P., 1999. Global changes in intensity of the Earth's magnetic field during the past 800 kyr. Nature 399, 249–252.
Hagstrum, J.T., Champion, D.E., 2002. A Holocene paleosecular variation record from ^{14}C-dated volcanic rocks in western North America Journal of Geophysical Research 107 (B1) , 8–1:8-14.

Hill, J.C., Driscoll, N.W., 2008. Paleodrainage on the Chukchi shelf reveals sea level history and meltwater discharge. Marine Geology 254, 129–151.
Hill, P.R., Blasco, S.M., Harper, J.R., Fissel, D.B., 1991. Sedimentation on the Canadian Beaufort Shelf. Continental Shelf Research 11 (8–10), 821–841.
Hughen, K.A., Baillie, M.G.L., Bard, E., Bayliss, A., Beck, J.W., Bertrand, C.J.H., Blackwell, P.G., Buck, C.E., Burr, G.S., Cutler, K.B., Damon, P.E., Edwards, R.L., Fairbanks, R.G., Friedrich, M., Guilderson, T.P., Kromer, B., McCormac, F.G., Manning, S.W., Bronk Ramsey, C., Reimer, P.J., Reimer, R.W., Remmele, S., Southon, J.R., Stuiver, M., Talamo, S., Taylor, F.W., van der Plicht, J., Weyhenmeyer, C.E., 2004. Marine04 Marine radiocarbon age calibration, 26–0 ka BP. Radiocarbon, 46, 1059–1086.
Keigwin, L.D., Donnelly, J.P., Cook, M.S., Driscoll, N.W., Brigham-Grette, J., 2006. Rapid sea-level rise and Holocene climate in the Chukchi Sea. Geology 34, 861–864.
King, J.W., Banerjee, S.K., Marvin, J.A., Özdemir, Ö., 1982. A comparison of different magnetic methods for determining the relative grain size of magnetite in natural materials: some results from lake sediments. Earth and Planetary Science Letters 59, 404–419.
King, J.W., Banerjee, S.K., Marvin, J., 1983. A new rock magnetic approach to selecting sediments for geomagnetic paleointensity studies: application to paleointensity for the last 4000 years. Journal of Geophysical Research 88, 5911–5921.
Kirschvink, J.L., 1980. The least-squares line and plane and the analysis of paleomagnetic data. Geophysical Journal of the Royal Astronomical Society 62, 699–718.
Korte, M., Constable, C.G., 2005. The geomagnetic dipole moment over the last 7000 years —new results from a global model. Earth and Planetary Science Letters 236, 348–358.
Korte, M., Constable, C.G., 2006. On the use of calibrated relative paleointensity records to improve millennial-scale geomagnetic field models. Geochemistry Geophysics Geosystems 7, Q09004.
Kotilainen, A.T., Saarinen, T., Winterhalter, B., 2000. High-resolution paleomagnetic dating of sediments deposited in the central Baltic Sea during the last 3000 years. Marine Geology 166, 51–64.
Laj, C., Kissel, C., Mazaud, A., Channell, J.E.T., Beer, J., 2000. North Atlantic Paleointensity Stack since 75 ka (NAPIS-75) and the duration of the Laschamp event. Philosophical Transaction of the Royal Society (London Series A) 358, 1009–1025.
Lund, S.P., 1996. A comparison of Holocene paleomagnetic secular variation records from North America. Journal of Geophysical Research 101, 8007–8024.
Lund, S.P., Banerjee, S.K., 1985. Late Quaternary paleomagnetic field variations from two Minnesota lakes. Journal of Geophysical Research 90, 803–825.
Mackereth, F.J.H., 1971. On the variation in the direction of the horizontal magnetization in lake sediments. Earth and Planetary Science Letters 12, 332–338.
Maher, A.B., Thompson, R., Hounslow, M.W., 1999. Introduction. In: Maher, A.B., Thompson, R. (Eds.), Quaternary Climates, Environments and Magnetism. Cambridge University press, United Kingdom.
Mazaud, A., 2005. User-friendly software for vector analysis of the magnetization of long sediment cores. Geochemistry Geophysics Geosystems 6, Q12006.
Nowacyzk, N.R., Harwart, S., Melles, M., 2001. Impact of early diagenesis and bulk particle grain size distribution on estimates of relative geomagnetic palaeointensity variations in sediments from Lama Lake, northern Central Siberia. Geophysical Journal International 145, 300–306.
Nowaczyk, N.R., Antonow, M., Knies, J., Spielhagen, R.F., 2003. Further rock magnetic and chonostratigraphic results on reversal excursions during the last 50 ka as derived from northern high latitudes and discrepancies in precise AMS ^{14}C dating. Geophysical Journal International 155 (3), 1065–1080.
Ortiz, J., Polyak, L., Greibmeir, J., Darby, D., Eberl, D., Naidu, S., Nof, D., 2009. Provenance of Holocene sediment on the Chukchi-Alaskan margin based on combined diffuse spectral reflectance and quantitative X-Ray Diffraction analysis. Global and Planetary Change 68, 73–84 (this issue).
Paillard, D., Labeyrie, L., Yiou, P., 1996. Macintosh program performs time-series analysis. Eos Trans. AGU 77, 379.
Peters, C., Dekkers, M.J., 2003. Selected room temperature magnetic parameters as a function of mineralogy, concentration and grain size. Physics and Chemistry of the Earth, Part A/B/C 28 (16–19), 659–667.
Phillips, R.L., Barnes, P., Hunter, R.E., Reiss, T.E., Rearic, D.M., 1988. Geologic Investigations in the Chukchi Sea, 1984, NOAA Ship SUVEYOR Cruise, Open-file Report 88-25. United States Department of the Interior Geological Survey, Menlo Park, California.
Pickart, R.S., Weingartner, T.J., Pratt, L.J., Zimmermann, S., Torres, D.J., 2005. Flow of winter-transformed Pacific water into the Western Arctic. Deep-Sea Research II 52, 3175–3198.
Polyak, L., Darby, D.A., Bischof, J.F., Jakobsson, M., 2007. Stratigraphic constraints on late Pleistocene glacial erosion and deglaciation of the Chukchi margin, Arctic Ocean. Quaternary Research 67, 234–245.
Reimer, P.J., Baillie, M.G.L., Bard, E., Bayliss, A., Beck, J.W., Bertrand, C., Blackwell, P.G., Buck, C.E., Burr, G., Cutler, K.B., Damon, P.E., Edwards, R.L., Fairbanks, R.G., Friedrich, M., Guilderson, T.P., Hughen, K.A., Kromer, B., McCormac, F.G., Manning, S., Bronk Ramsey, C., Reimer, R.W., Remmele, S., Southon, J.R., Stuiver, M., Talamo, S., Taylor, F.W., van der Plicht, J., Weyhenmeyer, C.E., 2004. IntCal04 Atmospheric radiocarbon age calibration, 26–0 ka BP. Radiocarbon 46, 1029–1058.
Saarinen, T., 1999. Paleomagnetic dating of Late Holocene sediments in Fennoscandia. Quaternary Science Reviews 18, 889–897.
Snowball, I., Sandgren, P., 2002. Geomagnetic field variations in northern Sweden during the Holocene quantified from varved lake sediments and their implications for cosmogenic nuclide production rates. The Holocene 12, 517–530.
Snowball, I., Sandgren, P., 2004. Geomagnetic field intensity changes in Sweden between 9000 and 450 cal BP: extending the record of "archeomagnetic jerks" by means of lake sediments and the pseudo-Thellier technique. Earth and Planetary Science Letters 227, 361–376.
Snowball, I., Zillén, L., Ojala, A., Saarinen, T., Sandgren, P., 2007. FENNOSTACK and FENNORPIS: varve dated Holocene paleomagnetic secular variation and relative paleointensity stacks for Fennoscandia. Earth and Planetary Science Letters 255, 106–116.
Stockhausen, H., Zolitschka, B., 1999. Environmental changes since 13,000 cal. BP reflected in magnetic and sedimentological properties of sediments from Lake Holzmaar (Germany). Quaternary Science Reviews 18, 913–925.
Stoner, J.S., St-Onge, G., 2007. Magnetic stratigraphy in paleoceanography: reversals, excursions, paleointensity, and secular variation. In: Hillaire-Marcel, C., deVernal, A. (Eds.), Proxies in Late Cenozoic Paleoceanography (Developments in Marine Geology), vol. 1. Elsevier, pp. 99–138.
Stoner, J.S., Jennings, A., Kristjánsdóttir, G.B., Dunhill, G., Andrews, J.T., Hardardóttir, J., 2007. A paleomagnetic approach toward refining Holocene radiocarbon-based chronologies: paleoceanographic records from the north Iceland (MD99-2269) and east Greenland (MD99-2322) margins. Paleoceanography 22, PA1209.
St-Onge, G., Stoner, J.S., Hillaire-Marcel, C., 2003. Holocene paleomagnetic records from the St. Lawrence Estuary, eastern Canada: centennial- to millennial-scale geomagnetic modulation of cosmogenic isotopes. Earth and Planetary Science Letters 209, 113–130.
St-Onge, G., Mulder, T., Piper, D.J.W., Hillaire-Marcel, C., Stoner, J., 2004. Earthquake and flood-induced turbidites in the Saguenay Fjord (Québec): a Holocene paleoseismicity record. Quaternary Science Reviews 23, 283–294.
St-Onge, G., Mulder, T., Francus, P., Long, B., 2007. Continuous physical properties of cored marine sediment. In: Hillaire-Marcel, C., deVernal, A. (Eds.), Proxies in Late Cenozoic Paleoceanography (Developments in Marine Geology), vol. 1. Elsevier, pp. 99–138.
Stuiver, M., Reimer, P.J., Reimer, R.W., 2005. Online Radiocarbon Calibration Program CALIB 5.0.2. http://calib.qub.ac.uk/calib/.
Syvitski, J.P.M., 1991. Towards an understanding of sediment deposition on glaciated continental shelves. Continental Shelf Research 11 (8–10), 821–842.
Tauxe, L., 1993. Sedimentary records of relative paleointensity: theory and practice. Reviews of Geophysics 31, 319–354.
Tauxe, L., Mullender, T.A.T., Pick, T., 1996. Potbellies, wasp-waists, and superparamagnetism in magnetic hysteresis. Journal of Geophysical Research 101, 571–583.
Thompson, R., Oldfield, F., 1986. Environmental Magnetism. George Allen and Unwin Ltd, London.
Turner, G.M., 1987. A 5000 year geomagnetic paleosecular variation record from western Canada. Geophysical Journal International 91 (1), 103–121.
Turner, G.M., Thompson, R., 1981. Lake sediment record of the geomagnetic secular variation in Britain during Holocene times. Geophysical Journal of the Royal Astronomical Society 65, 703–725.
Valet, J.-P., 2003. Time variations in geomagnetic intensity. Reviews of Geophysics 41 (1), 4.1–4.44.
Verosub, K.L., Mehringer, P.J., Waterstraat, P., 1986. Holocene secular variation in Western North America: paleomagnetic record from Fish lake, Harney county, Oregon. Journal of Geophysical Research 91 (B3), 3609–3623.
Weeks, R., Laj, C., Endigoux, L., Fuller, M., Roberts, A., Manganne, R., Blanchard, E., Goree, W., 1993. Improvements in long-core measurements techniques: applications in paleomagnetism and paleoceanography. Geophysical Journal International 114, 651–662.
Weingartner, T.J., Cavalieri, D.J., Aagaard, K., Sasaki, Y., 1998. Circulation, dense water formation and outflow on the northeast Chukchi Sea shelf. Journal Geophysical Research 103, 7647–7662.